

 Open access • Journal Article • DOI:10.1115/1.2819287

Air Entrainment in the Developing Flow Region of Plunging Jets—Part 2: Experimental — Source link

Peter D. Cummings, Hubert Chanson

Institutions: University of Queensland

Published on: 01 Sep 1997 - Journal of Fluids Engineering-transactions of The Asme (American Society of Mechanical Engineers)

Topics: Air entrainment, Jet (fluid), Bubble, Turbulent diffusion and Two-phase flow

Related papers:

- [Air Entrainment in the Developing Flow Region of Plunging Jets—Part 1: Theoretical Development](#)
- [Air Bubble Entrainment in Free-Surface Turbulent Shear Flows](#)
- [Gas entrainment by plunging liquid jets](#)
- [Air entrapment and air bubble dispersion at two-dimensional plunging water jets](#)
- [Air entrainment in free-surface flows](#)

Share this paper:    

View more about this paper here: <https://typeset.io/papers/air-entrainment-in-the-developing-flow-region-of-plunging-45pepboqnv>

Air Entrainment in the Developing Flow Region of Plunging Jets—Part 2: Experimental

P. D. Cummings

Maritime Engineer,
Kinhill Engineers,
299 Coronation Drive,
Brisbane QLD 4064,
Australia

H. Chanson

Senior Lecturer,
Fluid Mechanics,
Hydraulics and Environmental Engineering,
Department of Civil Engineering,
The University of Queensland,
Brisbane QLD 4072,
Australia

(Data Bank Contribution)*

When a water jet impinges a pool of water at rest, air bubbles may be entrained and carried away below the pool free surface: this process is called plunging jet entrainment. The study presents new experimental data obtained with a vertical supported jet. Distributions of air concentration and mean air-water velocity, and bubble chord length distributions measured in the developing shear layer are presented. The results indicate that the distributions of void fraction follow closely analytical solution of the diffusion equation. Further, the momentum shear layer and the air bubble diffusion layer do not coincide. Chord length data show a wide range of air bubble sizes and overall the experimental results suggest strong interactions between the entrained air bubbles and the momentum transfer mechanisms.

Introduction

When a falling nappe impinges a pool of water, air bubbles are entrained at the intersection of the jet with the receiving waters (Fig. 1). Large numbers of air bubbles are entrained into the turbulent shear flow. This process is called plunging jet entrainment. Plunging jet applications include plunging jet columns, drop structures along waterways, cooling system in power plants, plunging breakers and waterfalls.

In a first paper (Cummings and Chanson, 1997), the authors reviewed the current knowledge on the plunging jet entrainment. They showed that most researchers studied circular jets of small sizes, and few experiments described quantitatively the flow field below the free-surface of the receiving pool. It is the purpose of this paper to present new experimental results obtained with a vertical supported plunging jet. First, the experimental apparatus is described in details. Then experimental results of air concentration, mean air-water velocities, and chord length distributions are presented. In a later part, the results are discussed and compared with other data.

Experimental Apparatus

Plunging Jet Apparatus. The experimental apparatus consists of a fresh water planar jet issuing from a 0.269-m \times 0.012-m slot nozzle and plunging into a 0.3-m wide (Fig. 1). The receiving channel is 1.8-m deep with glass walls (10-mm thick). The supported-jet nozzle is made of 6-mm thick PVC with lateral perspex windows for flow visualisation. The jet support length is 0.35 m and the angle of the support with the horizontal was 89-degrees for all experiments. The water supply (Brisbane tap water) comes from a constant-head tank with a constant water level of 12.9 m above the nozzle. The experiment provides average jet velocities from 0.3 to 9 m/s.

* Data have been deposited to the JFE Data Bank. To access the file for this paper, see instructions on p. 738 of this issue.

Contributed by the Fluids Engineering Division for publication in the JOURNAL OF FLUIDS ENGINEERING. Manuscript received by the Fluids Engineering Division December 5, 1995; revised manuscript received April 11, 1997. Associate Technical Editor: O. C. Jones.

The discharge was measured with orifice meters. The error on the discharge measurement was less than 1%.

Instrumentation. In the free-falling jet, clear water jet velocities and turbulent velocity, fluctuations (in clear-water flows) were measured with a Pitot tube connected to a pressure transducer (Validyne™ DP15, diaphragm ranges 2.2 to 22 kPa, accuracy 0.25 percent of full-scale). The transducer was scanned at 500 Hz and the accuracy of the clear-water velocity data was normally estimated as: $\Delta V/V =$ one percent. At very-low velocity (e.g., $V < 0.5$ m/s), measurements with the Pitot tube oriented vertically could mount up to 15 percent.

Two conductivity probes were used to record the air-water flow characteristics. A single-tip conductivity probe (inner electrode \varnothing : 0.35 mm, outer electrode \varnothing : 1.42 mm) was used to perform air concentration measurements only. A two-tip conductivity probe was used to record simultaneously the air concentration and air-water velocity. The two tips were aligned in the direction of the flow. Each tip is identical and has an internal concentric electrode ($\varnothing = 25$ μ m, Pt) and an external stainless steel electrode of 200 μ m diameter. Both conductivity probes are excited by an air bubble detector (Ref. AS25240). This electronic system was designed with a response time less than 10 μ s and it was calibrated with a square wave generator. Most measurements were recorded with a scan rate of 40 kHz per channel. The analysis of conductivity probe data provided the void fraction (i.e., air concentration), mean air-water interface velocity and chord length distributions at various positions within the developing shear layer.

The error on the air concentration (void fraction) measurements was estimated as: $\Delta C/C = 2$ percent for $5 < C < 95$ percent, $\Delta C/C \sim 0.001/(1 - C)$ for $C > 95$ percent, and $\Delta C/C \sim 0.001/C$ for $C < 5$ percent. The mean air-water velocities, recorded using the double-tip conductivity probe, were computed with a cross-correlation technique. The analysis of the velocity field and chord length distributions implies no slip between the air and water phases. The error on the mean air-water velocity measurements was estimated as: $\Delta V/V =$ five percent for $5 < C < 95$ percent, $\Delta V/V = 10$ for $1 < C < 5$ and $95 < C < 99$ percent. With the two-tip conductivity probe, the minimum detectable bubble chord length was about 100 μ m.

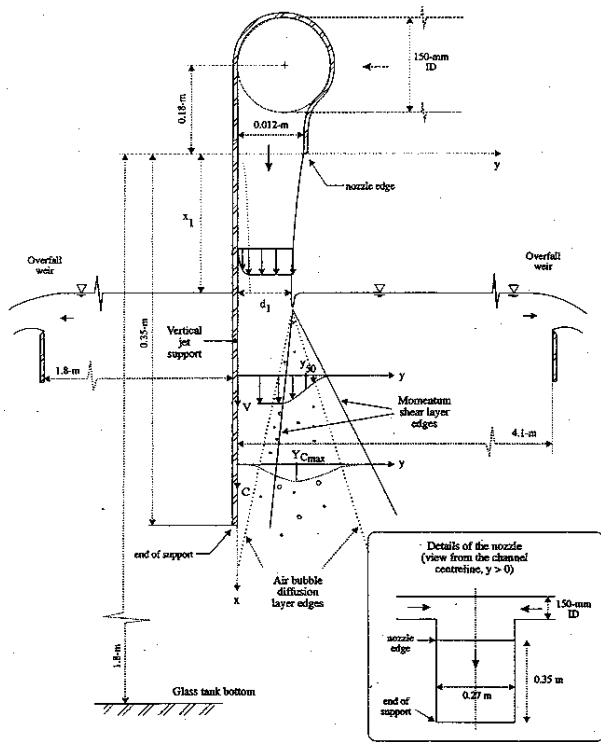


Fig. 1 Sketch of the vertical supported jet experiment

in a 1-m/s flow and 450 μm in a 9-m/s jet based upon a data acquisition frequency of 40 kHz per channel.

Measurements were taken on the channel centreline. The displacement of the probes in the direction normal to the jet support and along the jet direction were controlled by two identical scale-verniers. The error in the longitudinal and perpendicular positions of the probes is less than 0.25 mm in each direction.

Additional measurements were performed using high speed photographs with a flash speed of 33 μs (e.g., Chanson and Cummings, 1994) and high-speed video camera images with a shutter speed of 500 μs .

Calibration and Validation of the Measurement Techniques. Several calibration tests were performed to compare the single-tip and double-tip conductivity probes. Identical ex-

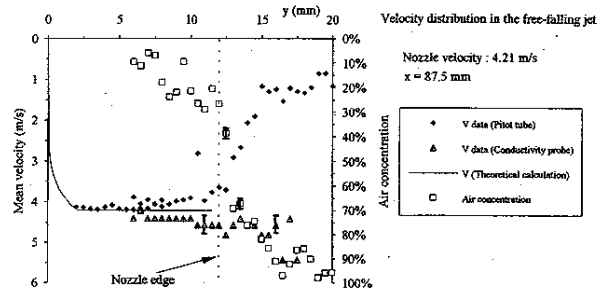


Fig. 2(a) Nozzle velocity: 4.21 m/s

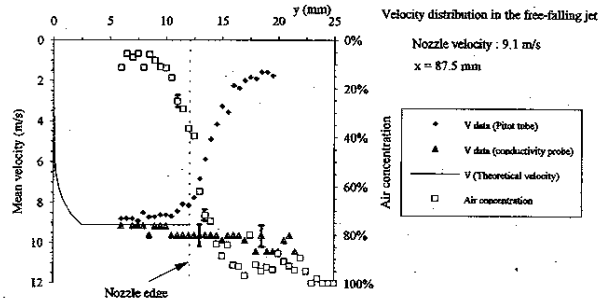


Fig. 2(b) Nozzle velocity: 9.1 m/s

Fig. 2 Distributions of air concentration and mean air-water velocity the free-falling jet—comparison between experimental data and calculations

periments were performed with both the single-tip and conductivity probes. In each case, identical air concentration data were observed (within the accuracy of the data) suggesting that the probe diameter has little effect on the void fraction measurement.

To validate the double-tip probe measurement technique, measurements were performed within the free-falling supported jet (i.e., $x < x_1$). Velocities were recorded using both the dual tip conductivity probe and Pitot tube. The tips of each probe were located at the same location for comparison. The data were compared with theoretical calculations: ideal-fluid flow calculation outside of the boundary layer and power law velocity distribution within the developing turbulent boundary layer. Figure 2 presents typical results. The agreement between the two probes and the theoretical calculation are within the accuracy of the measurement techniques.

Nomenclature

C = air concentration defined as the volume of air per unit volume of air and water; it is also called void fraction
 C_{max} = maximum air concentration in the air bubble diffusion layer
 D_t = turbulent diffusivity (m^2/s)
 D^* = dimensionless turbulent diffusivity: $D^* = D_t/(V_1 d_1)$ for two-dimensional shear flow
 d = flow depth or jet thickness (m) measured perpendicular to the flow direction
 d_1 = jet thickness (m) at the impact of a supported plunging jet with the receiving pool of liquid
 g = gravity constant: $g = 9.80 \text{ m/s}^2$ in Brisbane, Australia

K = integration constant in Goertler's (1942) solution of the motion equation in a free shear layer
 Q = volume discharge (m^3/s)
 q = volume discharge per unit width (m^2/s)
 u = dimensionless variable
 V = velocity (m/s)
 V_1 = mean flow velocity (m/s) at jet impact
 W = channel width (m)
 x = distance along the flow direction (m)
 x_1 = distance (m) between the channel intake and the impact flow conditions
 y = distance (m) measured normal to the flow direction

$Y_{C_{\text{max}}}$ = distance (m) normal to the bottom where $C = C_{\text{max}}$
 y_{50} = distance (m) normal to the flow direction where $V = 0.5V_1$
 ν_T = eddy viscosity (m^2/s) or momentum exchange coefficient
 ω = vorticity (s^{-1})
 \varnothing = diameter (m)
 Δ = error

Subscript

air = air flow
 w = water flow
 x = component in the x -direction
 y = component in the y -direction
 1 = impact flow conditions

Further comparisons between Pitot tube and conductivity probe data were performed during each experiment. Velocities were recorded as close as possible of the support, and the data were compared successfully with the ideal-fluid flow velocity deduced from the continuity and Bernoulli equation. Typical results are shown in Figs. 3 and 4. Additional verifications were conducted by checking the continuity equation for water at each cross-section (i.e., $q_w = \int_0^{\infty} (1 - C)Vdy$).

Experimental Flow Conditions. A large number of experiments were performed with jet impact velocities ranging from 0.5 to 9 m/s. The entire flow characteristics were recorded for two jet velocities (Table 1). For most experiments, the vertical jet impacted the receiving pool of water at 0.09-m below the jet nozzle. The impact flow conditions were not fully-developed and the ratio of the boundary layer thickness over jet thickness δ/d_1 was less than 0.2.

During the experiments, the plunging jet was unsteady and fluctuating while the probes were fixed and did not follow the fluctuations of the flow (e.g., fluctuations of pool free-surface). As a result, the data (e.g., Figs. 3 and 4) exhibit a greater scatter than the probe accuracy, reflecting the unsteady fluctuating nature of the investigated flow.

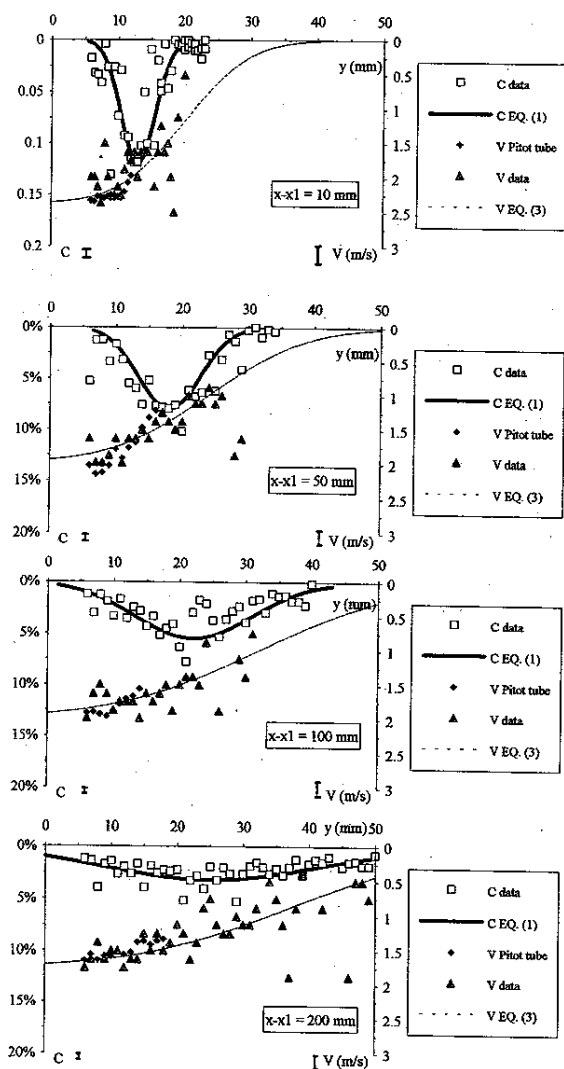


Fig. 3 Distributions of air concentration and mean air-water velocity in the developing flow region of vertical supported plunging jets—comparison between Eqs. (1) and (3) and experimental data (impact velocity $V_1 = 2.39$ m/s)

Full details of the experimental apparatus and instrumentation, and experimental results are reported in Cummings (1996). An earlier series of experiments performed in the same facility was reported in Chanson (1995).

Experimental Results and Discussion

Air Concentration Distributions. Figures 3 and 4 present some experimental results for two jet impact velocities and at several locations below the impingement point. Both air concentration and velocity profiles are plotted as functions of the distance normal to the jet support.

For a two-dimensional supported jet, the air concentration data followed closely an analytical solution of the diffusion equation (Cummings and Chanson, 1997):

$$C = \frac{Q_{air}}{Q_w} \frac{1}{\sqrt{4\pi D^* \frac{x-x_1}{d_1}}} \left(\exp\left(-\frac{1}{4D^*} \frac{\left(\frac{y}{d_1} - 1\right)^2}{\frac{x-x_1}{d_1}}\right) + \exp\left(-\frac{1}{4D^*} \frac{\left(\frac{y}{d_1} + 1\right)^2}{\frac{x-x_1}{d_1}}\right) \right) \quad (1a)$$

where C is the air concentration defined as the volume of air per unit volume of air and water, x is the longitudinal jet direction, x_1 is the impact point location, y is the normal direction, d_1 is the impact jet thickness of supported jet, Q_{air} is the volume air flow rate and D^* is a dimensionless diffusivity ($D^* = D/(V_1 d_1)$ for vertical supported jet). Equation (1a) was compared successfully with experimental data (e.g., Figs. 3 and 4).

In the developing air-water flow region (i.e., $C(y=0) = 0$), Eq. (1a) can be simplified as:

$$C = \frac{Q_{air}}{Q_w} \frac{1}{\sqrt{4\pi D^* \frac{x-x_1}{d_1}}} \exp\left(-\frac{1}{4D^*} \frac{\left(\frac{y}{d_1} - 1\right)^2}{\frac{x-x_1}{d_1}}\right) \quad \text{developing air-water flow region} \quad (1b)$$

Mean Air-Water Velocity Distributions. Downstream of the intersection of the free-falling jet with the receiving pool of water, a free-shear layer develops (Fig. 1). For monophasic flows, Goertler (1942) solved the equation of motion for a plane shear layer assuming a constant eddy viscosity ν_T across the shear layer:

$$\nu_T = \frac{1}{4K^2} (x - x_1) V_1 \quad (2)$$

where K is a constant. The solution in the first approximation yields (Rajaratnam, 1976, Schlichting, 1979):

$$\frac{V}{V_1} = \frac{1}{2} \left(1 + \operatorname{erf} \left(\frac{K(y - y_{50})}{x - x_1} \right) \right) \quad (3)$$

where y_{50} is the location where $V = V_1/2$ and erf is the error function:

$$\operatorname{erf}(u) = \frac{2}{\sqrt{\pi}} \int_0^u \exp(-u^2) du \quad (4)$$

Equation (3) is an analytical solution of the motion equation developed for two-dimensional monophasic flow. In air-water flows, the presence of air bubbles within the shear

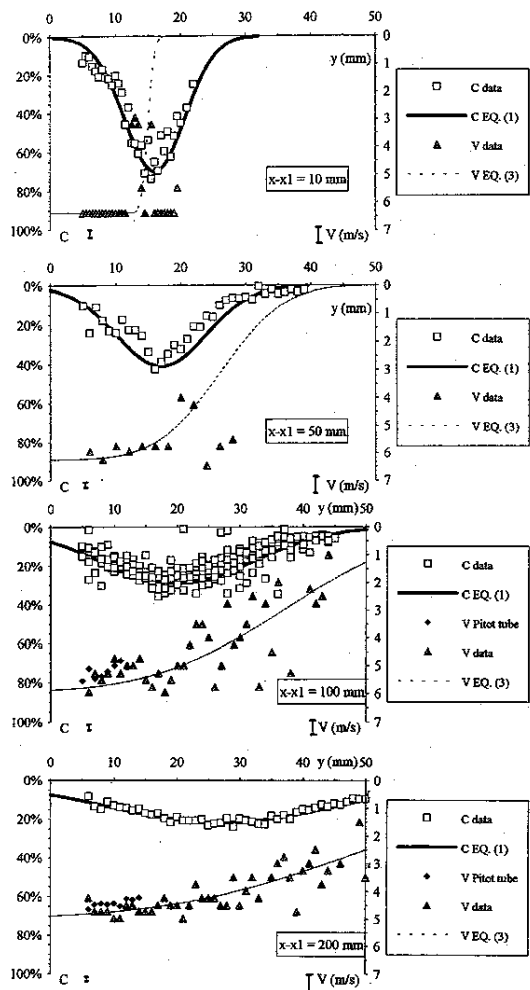


Fig. 4 Distributions of air concentration and mean air-water velocity in the developing flow region of vertical supported plunging jets—comparison between Eqs. (1) and (3) and experimental data (impact velocity $V_1 = 6.14$ m/s).

layer is expected to affect the shear flow which in turn affects the diffusion of air bubbles. In Figs. 3 and 4 the mean velocities of the air-water mixture (experimental data) are compared with Eq. (3). Figures 3 and 4 indicate that the air-water velocity profiles have the same shape as in monophasic flows.

In the air-water shear layer of vertical supported jets, the authors estimated $K = 10.6$ and 6.3 for $V_1 = 2.39$ and 6.14 m/s, respectively. In comparison, for monophasic shear flows, Rajaratnam (1976) and Schlichting (1979) deduced $K = 11$ and 13.5 . As the rate of expansion of the shear layer is proportional to $1/K$, the new results suggest that the air bubbles cause an increase in the expansion rate for the 6.14 -m/s jet.

Remarks. In Figs. 3 and 4, the velocity conductivity probe data are compared with Pitot tube measurements in the low air content region close to the support.

Note also that, during the experiments, the plunging jet was unsteady and the free-surface level fluctuating while the probes were fixed to the channel. Hence, the experimental results (e.g., Figs. 3 and 4) exhibit more scatter than the accuracy of the probes.

Chord Length Distributions. At each position $\{x, y\}$ below the entrainment point, the chord length¹ distributions were also computed. A dual tip conductivity probe, used to measure air bubble size characteristics, detects only the bubble chord lengths. If the bubbles are small (i.e. less than 0.1 mm), the bubble diameter probability distribution can be deduced from the bubble chord probability distribution by assuming that all the bubbles are spherical or ellipsoidal (e.g., Heringe and Davis, 1976, Clark and Turton, 1988). In the present bubbly free-shear-layer flow, video pictures and still camera photographs showed the entrainment of large bubbles with a large variety of shapes (Cummings, 1996). For these reasons only the bubble chord data are presented here.

In Fig. 5 the bubble chord probability histograms are shown. The histogram columns represent each the probability of a bubble chord length in one millimetre intervals (e.g., the probability of a chord length from 2.0 to 3.0 mm is represented by the column labeled 3). The histograms describe all the bubble detected across the shear layer width at depths $(x - x_1) = 10, 50, 100$ and 200 mm.

First, note the broad range of bubble chord lengths: i.e., from less than 0.1 mm to more than 30 mm. The observations of bubble chord length indicated consistently a broad range of bubble sizes, extending over several orders of magnitude.

Second, Figs. 5(a) and 5(b) show clearly the existence of large chord-length bubbles at $(x - x_1) = 10$ -mm (i.e., very close to the entrainment point). Further downstream (i.e., $(x - x_1) = 100$ to 200 mm), most large chord length bubbles have disappeared presumably by a bubble breakage process in the turbulent shear flow. This bubble breakage is confirmed by high speed video and photographic observations, showing that the bubbles can be entrained in the form of elongated air packets which break later within the free shear layer. Bubble de-trainment is unlikely to account for the disappearance of the larger bubbles so close to the entrainment point.

Discussion. For a two-dimensional shear layer, the vorticity ω can be deduced from the velocity profile (Eq. (3)) by neglecting the term $\partial V_y / \partial x$. In dimensionless terms, it yields:

$$\frac{\omega d_1}{V_1} = -\frac{1}{2} \frac{d_1}{V_1} \frac{\partial V_x}{\partial y} = -\frac{1}{2} \frac{1}{\sqrt{4\pi} \frac{\nu_T}{V_1 d_1} \frac{x - x_1}{d_1}} \times \exp\left(-\frac{1}{4} \frac{\nu_T}{V_1 d_1} \frac{(y - y_{50})^2}{d_1} \frac{x - x_1}{d_1}\right) \quad (5)$$

Equation (5) is very similar to Eq. (1b). It implies that, for plane shear layers, the advective diffusion of vorticity is of similar shape as that of air bubble (Eqs. (1a) and (1b)). The diffusion processes of air bubbles and vorticity are primarily defined by their dimensionless diffusivity (i.e., $D_r / (V_1 d_1)$ and $\nu_T / (V_1 d_1)$, respectively) and their axis of symmetry (i.e., $Y_{C_{max}}$ and y_{50} , respectively).

Air Diffusion Layer and Momentum Shear Layer. First it is important to note that the momentum shear layer (as described by the mean air-water velocity field) does not coincide with the air bubble diffusion layer. Further, with vertical supported plunging jets, the new experiments showed consistently that $1 - y_{50} > Y_{C_{max}}$ where $Y_{C_{max}}$ is the location where the air

¹ Length of the straight line connecting the two intersections of the air-bubble free-surface with the tip of the probe as the bubble is transixed by the probe sharp-edge.

Table 1 Experimental values of turbulent diffusivity and eddy viscosity at vertical supported jets

Ref. (1)	Run (2)	V_1 m/s (3)	d_1 m (4)	x_1 m (5)	$\frac{q_{air}}{q_w}$ (6)	$\frac{D_t}{V_1 d_1}$ (7)	$\frac{\nu_T}{V_1 d_1}$ (8)	Comments (9)
Chanson (1995)	F1	2.36	0.0102	0.090	N/A	0.039	N/A	Two-dimensional supported jet. $W = 0.269$ m.
	F2	4.06	0.0118	0.090	N/A	0.018	N/A	
	F3	5.89	0.0122	0.090	N/A	0.037	N/A	
	F4	8.0	0.012	0.090	N/A	0.061	N/A	
	F5	9.0	0.012	0.090	N/A	0.053	N/A	
Present study	2-m/s	2.39	0.010	0.0875	0.057	0.039	0.011	Two-dimensional supported jet. $W = 0.269$ m.
	6-m/s	6.14	0.0117	0.0875	0.543	0.038	0.027	

Notes:

N/A: not available.

$q_{air} = \int_0^W C V dy$, where both C and V were measured locally.

W : plunging jet width.

concentration is maximum (i.e. $C = C_{max}$) at a given cross-section (Fig. 1).

For monophasic flows, Rajaratnam (1976) quoted:

$$\left(\frac{y_{50} - d_1}{x - x_1} \right)_{\text{monophasic}} = +0.041 \quad \text{monophasic shear layer} \quad (6)$$

while the authors' results suggest that:

$$\left(\frac{y_{50} - d_1}{x - x_1} \right)_{\text{air-water}} = +0.226 + 0.024 V_1 \quad \text{air-water shear layer} \quad (7)$$

where V_1 is in m/s. In comparison, the symmetry line of air bubble diffusion layer (i.e. $y = Y_{C_{max}}$) was estimated as:

$$\left(\frac{Y_{C_{max}} - d_1}{x - x_1} \right)_{\text{air-water}} \sim +0.10 \quad (\text{Chanson, 1995, } 2 < V_1 < 9 \text{ m/s}) \quad (8)$$

Basically the present air-water flow data (Eqs. (7) and (8)) imply that the symmetry lines of monophasic shear layer, air diffusion cone and air-water shear layer satisfy: $(y_{50})_{\text{monophasic}} < Y_{C_{max}} < (y_{50})_{\text{air-water}}$.

Turbulent Diffusivity and Eddy Viscosity. There is little information on the turbulent diffusivity. Chanson (1995) reported some air bubble diffusivity values. These results are compared with the authors' results in Table 1. Momentum exchange coefficients observed in the air-water shear layer are reported also. In each case, the values of D_t and ν_T were determined from the best fit of the data (Table 1).

For the small number of results presented in Table 1, it is worth noting that the dimensionless turbulent diffusivity and eddy viscosity are of the same order of magnitude. Further the turbulent diffusivity of air bubbles tends to be larger than the momentum exchange coefficient for the two series of experiments (Table 1, columns 6 and 7).

Overall Discussion of Plunging Jet Flows

Plunging jet entrainment takes place when the jet impact velocity exceeds a critical velocity. This characteristic velocity is a function of the jet turbulence. For small jet velocities (larger than the critical velocity), air is entrained in the form of individual air pockets and bubbles. At larger jet velocities, large air packets are entrained and broken up subsequently in the shear flow.

The near-flow field is characterized by a developing shear layer and an air diffusion layer (Fig. 1). New experimental results with the vertical supported jet have shown that these layers do not coincide. Below the impingement point, the air entrainment is primarily an advection-diffusion process (Cummings and Chanson, 1997). And most air is entrained in the region of high-velocity ($y < y_{50}$). Although the velocity distribution has the same shape as for monophasic flows, its quantitative parameters (ν_T , y_{50}) are affected by the air entrainment process.

The interactions between the air bubble diffusion and the shear flow are significant. The presence of bubbles within the shear layer modifies the momentum transfer between the high-velocity jet core and the surrounding fluid (at rest at infinity). And the turbulent shear flow contributes to the bubble breakage, leading to a broad spectrum of bubble sizes in the shear layer (Fig. 5).

JFE Data Bank Contribution

Plunging jet experiments were performed using a two-dimensional vertical supported jet facility. The apparatus consists of a glass tank with a depth of 1.8 m, a width of 0.30 m and a length of 3.6 m. A PVC rotatable slot nozzle supplies a planar supported jet, 0.27 m wide and 0.012 m thick. The length of

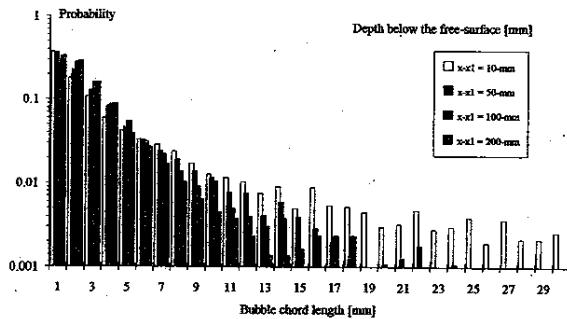


Fig. 5(a) Impact velocity $V_1 = 2.35$ m/s

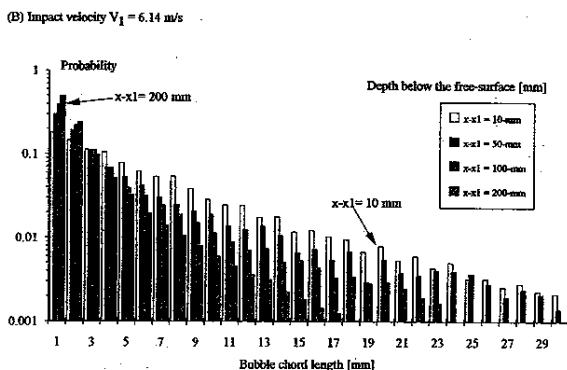


Fig. 5(b) Impact velocity $V_1 = 6.14$ m/s

Fig. 5 Bubble chord length probability histogram for a vertical supported jet at various cross-sections below the entrainment point

the plate that supported the jet was 0.35 m and its inclination with the horizontal was 89 degrees for all experiments. The water supply comes from a constant head tank, which has a constant water level of 12.9 m above the nozzle.

A summary of the experiments is presented in section 2 before the full set of data (Sections 3 and 4). The full set of experimental data was first published in: Chanson, H., 1995, "Air bubble Entrainment in Free-Surface Turbulent Flows. Experimental Investigations," Report CH 46/95, Department of Civil Engineering, University of Queensland, Australia, June, 368 pages (ISBN 0 86776 611 5).

Conclusion

New experiments were performed in the developing flow region of a vertical supported plunging jet. The air-water shear flow was investigated. The main results of the study are:

1 In two-dimensional plunging jet flows, the distributions of air concentration follow closely analytical solutions of the diffusion equation (Cummings and Chanson, 1997). And the velocity profiles have the same shape (Eq. (3)) as monophasic flows. But the data show that the rate of spread of the shear layer is enhanced by the entrained bubbles for the 6.1-m/s jet experiment.

2 The results show consistently that the air bubble diffusion and momentum exchange layers do not coincide. The momentum shear layer is shifted away from the jet support compared to monophasic flows, and air bubble diffusion takes place predominantly in the inner part of the shear layer: i.e., $Y_{C_{max}} < y_{50}$.

3 Chord length data show a broad range of entrained bubble sizes. The measurements show also the entrainment of some large air pockets which are subsequently broken into smaller air bubbles as they are entrained within the shear flow.

Overall, the developing flow region of plunging jets is subjected to strong interactions between the entrained air bubbles and the momentum transfer mechanism.

Acknowledgments

The authors want to thank particularly Professor C. J. Apelt, University of Queensland who supported this project since its beginning. They acknowledge the support of the Department of Civil Engineering at the University of Queensland which provided the experimental facility and the financial support of Australian Research Council (Ref. No. A89331591). The first author was supported by an Australian Postgraduate Award during his Ph.D. thesis.

The authors appreciate the helpful comments of the anonymous reviewers and of the associated technical editor, Professor O. C. Jones.

References

- Chanson, H., and Cummings, P. D. (1994). "An Experimental Study on Air Carryunder due to Plunging Liquid Jet—Discussion," *International Journal of Multiphase Flow*, Vol. 20, No. 3, pp. 667–770.
- Chanson, H., 1995, "Air Bubble Entrainment in Free-surface Turbulent Flows. Experimental Investigations," Report CH46/95, Dept. of Civil Engineering, University of Queensland, Australia, June, 368 pages.
- Clark, N. N., and Turton, R., 1988, "Chord Length Distributions Related to Bubble Size Distributions in Multiphase Flows," *International Journal of Multiphase Flow*, Vol. 14, No. 4, pp. 413–424.
- Cummings, P. D., 1996, "Aeration due to Breaking Waves," Ph.D. thesis, Dept. of Civil Engrg., University of Queensland, Australia.
- Cummings, P. D., and Chanson, H. 1997, "Air Entrainment in the Developing Flow Region of Plunging Jets. Part 1," *ASME JOURNAL OF FLUIDS ENGINEERING*, published in this issue pp. 597–602.
- Goertler, H., 1942, "Berechnung von Aufgaben der freien Turbulenz auf Grund eines neuen Näherungsansatzes," *Zeitschrift für angewandte Mathematik und Mechanik*, Vol. 22, pp. 244–254 (in German).
- Herrige, R. A., and Davis, M. R., 1976, "Structural Development of Gas-Liquid Mixture Flows," *Journal of Fluid Mechanics*, Vol. 73, pp. 97–123.
- Rajaratnam, N., 1976, *Turbulent Jets*, Elsevier Scientific, Development in Water Science, 5, New York.
- Schlichting, H., 1979, *Boundary Layer Theory*, McGraw-Hill, New York, 7th edition.